Supplemental Figure 1

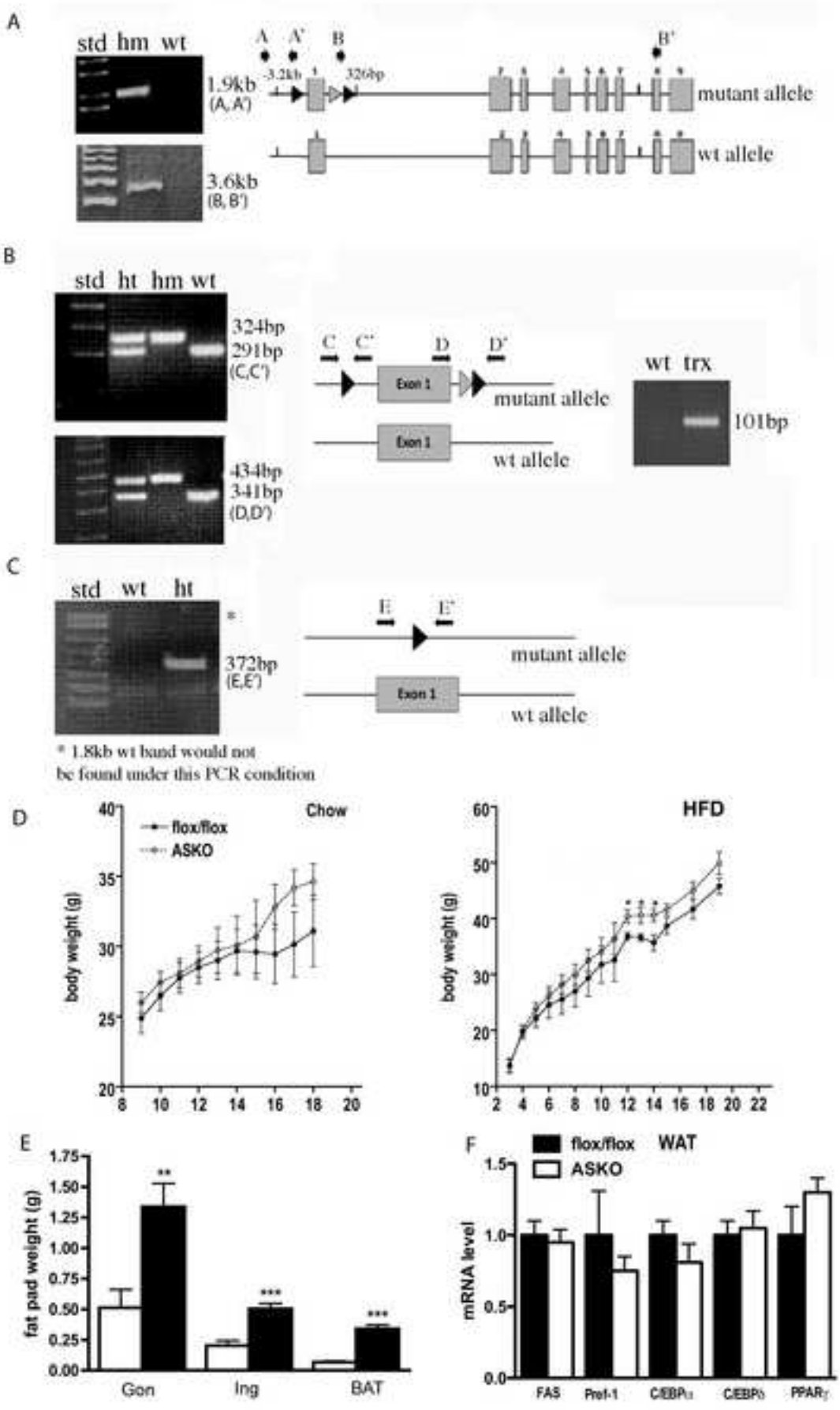

Supplemental Figure 2

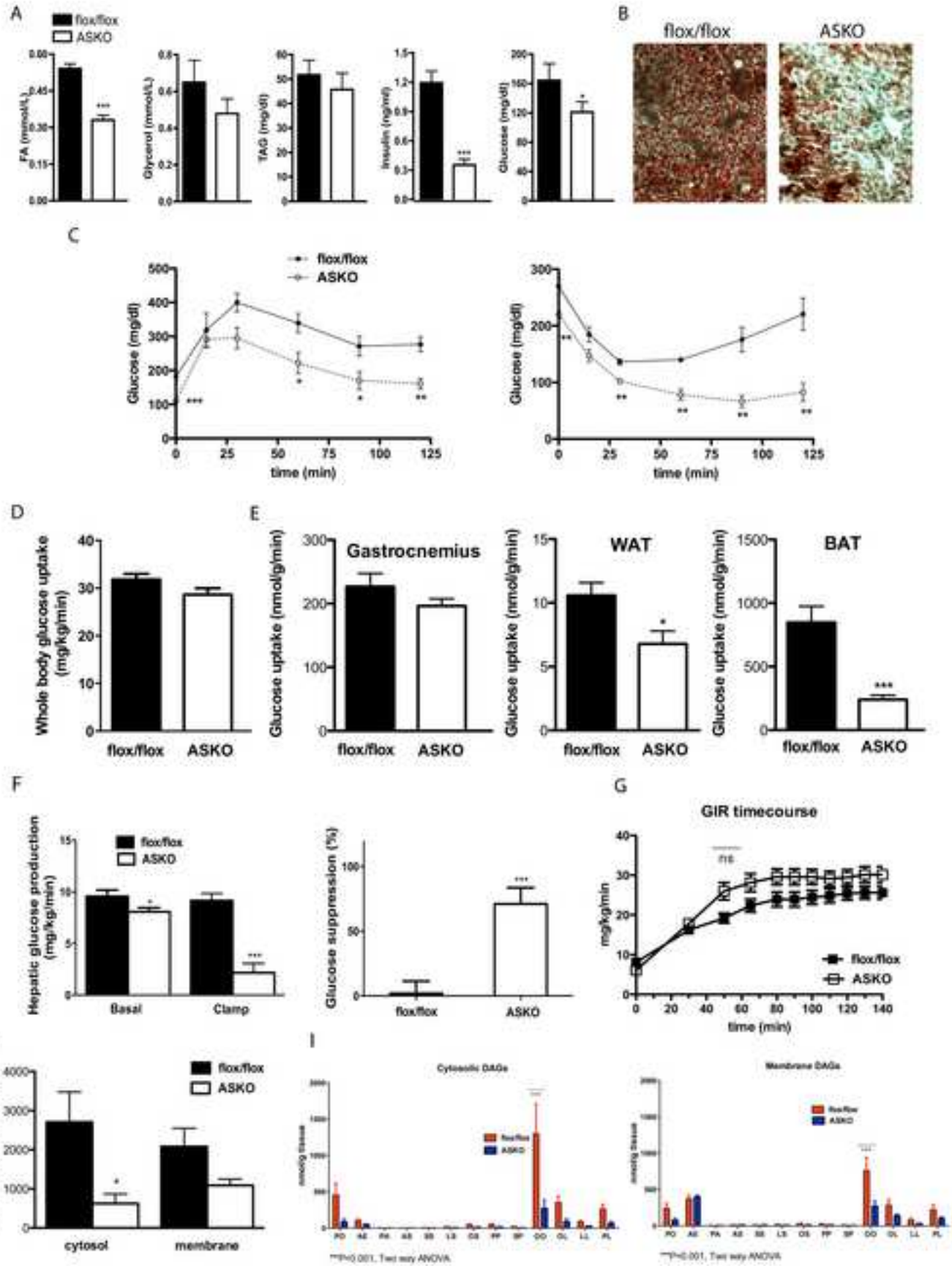

Supplemental Figure 3

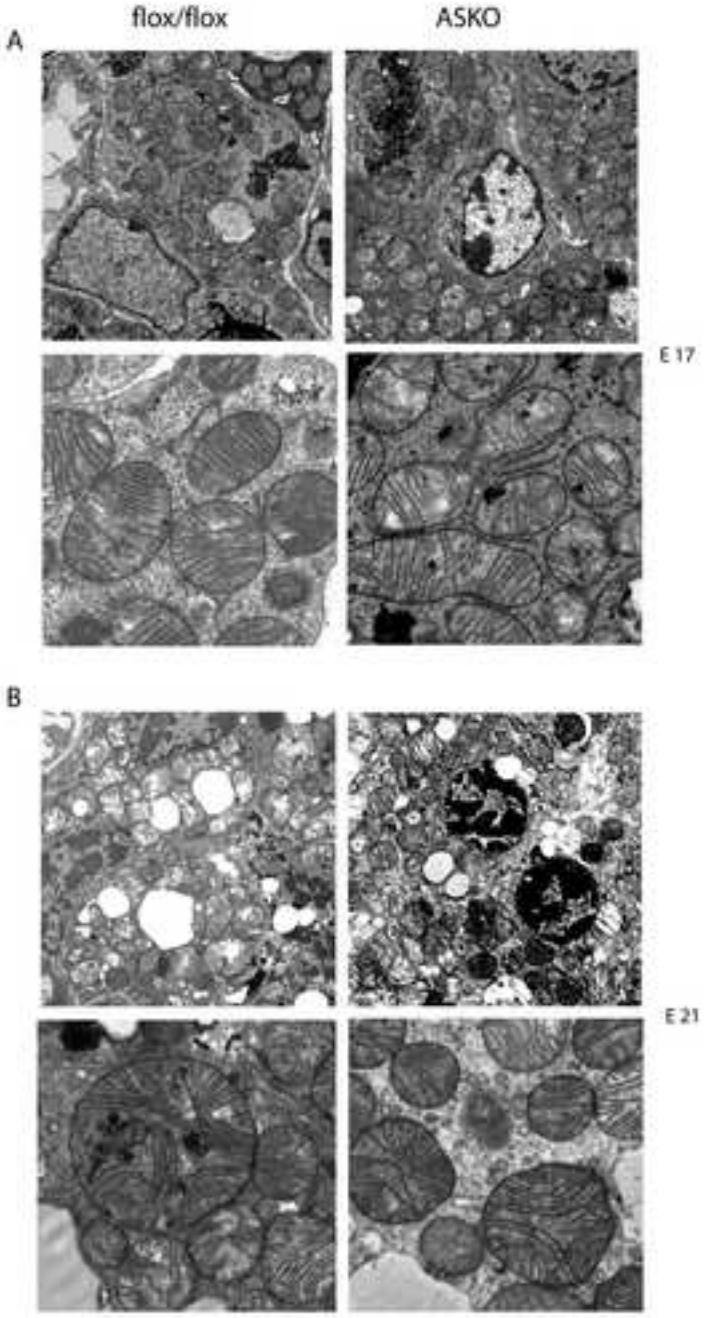

Supplemental Figure 4

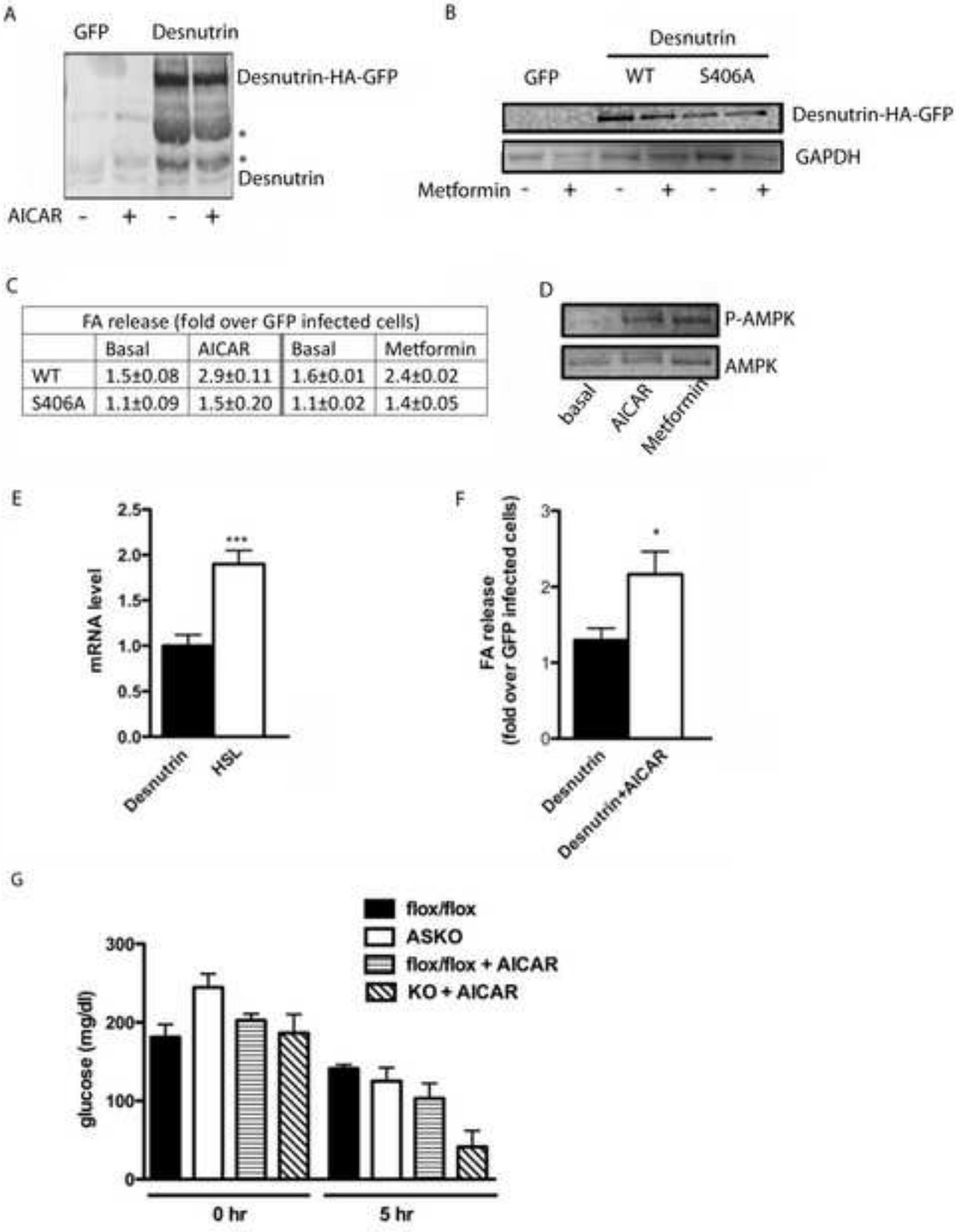

FA release (fold over GFP infected cells)				
	Basal	AICAR	Basal	Metformin
WT	1.5±0.08	2.9±0.11	1.6±0.01	2.4±0.02
S406A	1.1±0.09	1.5±0.20	1.1±0.02	1.4±0.05

Supplemental Table 1

Gene name	Applied Biosystem reference number
Pref-1	Mm00494478_m1
C/EBPα	Mm00514283_s1
C/EBPδ	Mm00514291_s1
PPARγ	Mm00440945_m1
ATP5β	Mm00443967_g1
COX4	Mm01250094_m1
CPT1β	Mm01308160_m1
phyH	Mm01333210_m1
Cidea	Mm00432554_m1
PPARα	Mm00440939_m1
UCP1	Mm01244861_m1
RIP140	Mm01343437_m1
CtBP1	Mm00516350_m1
Igfbp3	Mm00515156_m1
DPT	Mm00498111_m1
HOXC9	Mm00433972_m1
Tcf21	Mm00448961_m1
GAPDH	Mm99999915_g1
Esr1	Mm00433149_m1
Nr1h3	Mm00443454_m1

Figure S1. Generation of desnutrin-ASKO mice and increased adiposity of desnutrin-ASKO mice. A) PCR verification for homologous recombination. B) Flp recombination for removal of puromycin. Transgenic Cre insertion was verified by PCR using tail DNA (right). C) Verification of Cre recombination using adipose tissue DNA for removal of exon 1. Ht; heterozygous, hm; homozygous, wt; wild-type, trx; transgenic for Cre. D) Body weights of male flox/flox and desnutrin-ASKO mice on a chow diet (left) (n=12) or a HFD (right) (n=10). E) Fat pad weights of male flox/flox and desnutrin-ASKO littermates on a chow diet at 20 wks of age (n = 8). F) RT-qPCR for the expression of markers for differentiation in WAT from flox/flox and desnutrin-ASKO mice. Data are expressed as means ± SEM. *P < 0.05, ***P < 0.001

Figure S2. Desnutrin-ASKO mice have improved hepatic insulin sensitivity with decreased DAG levels. A) Serum parameters from fasted desnutrin-ASKO mice (n=6-8). B) Cryosections of frozen livers stained with Oil red O and nuclei stained with hematoxylin. C) Glucose and insulin tolerance tests (GTT (left) and ITT (right)) from 16-wk old male mice on a HFD (n=6). D) Whole body and E) tissue specific insulin-stimulated glucose uptake and F) hepatic glucose production (left) and percent hepatic glucose suppression (right) determined from hyperinsulinemic-euglycemic clamp experiments on desnutrin-ASKO mice and flox/flox littermates. G) Glucose infusion rate (GIR) during the hyperinsulinemic euglycemic clamp in 16-wk old male flox/flox and ASKO mice on a HFD. H) Total DAG levels in livers of flox/flox and desnutrin-ASKO mice (n=6). I) Cytosolic (left) and membrane (right) DAG species from the livers of 16 wk old HFD-fed mice. DAG species are abbreviated as two contributing fatty acyl groups. S, stearoyl; O, oleoyl; L, linoleoyl; P, palmitoyl; A, Eicosatetraenoyl, E, Eicosapentaenoyl. Data are expressed as means ± SEM. *P < 0.05, **P < 0.01, ***P < 0.001

Desnutrin-ASKO mice exhibit impaired lipolysis and increased adiposity. Since adiposity is positively correlated with insulin resistance, we postulated that these mice might be more insulin resistant. On the other hand, since FAs are know to exert lipotoxic effects that disrupt insulin signaling, the impaired lipolysis in desnutrin-ASKO mice may protect these mice from HFD induced insulin resistance (Samuel et al., 2010). Consistent with blunted adipocyte lipolysis, we found that fasting serum FA levels were decreased by 39% in desnutrin-ASKO mice (Figure S2A). Furthermore, fasting levels of both glucose and insulin were decreased in desnutrin-ASKO mice on a HFD (Figure S2A). While we found no difference in lipid staining with Oil Red O in skeletal muscle (data not shown), we found less staining in the liver of desnutrin-ASKO mice, revealing decreased ectopic TAG storage, potentially due to lower circulating FA levels (Figure S2B). We also found that desnutrin-ASKO mice had improved glucose clearance during a GTT (Figure S2C, left). During an ITT, desnutrin-ASKO mice exhibited a prolonged response to insulin compared to flox/flox mice (Figure S2C, right). We also performed a hyperinsulinemic-euglycemic clamp with radioisotope-labeled glucose infusion in HFD-fed flox/flox and desnutrin-ASKO mice (Figure S2G). The steady state glucose infusion rate during the clamp and whole body glucose uptake were unchanged in desnutrin-ASKO mice (Figure S2D and G). Skeletal muscle 2-deoxyglucose uptake was also not different (Figure S2E, left). Notably, glucose uptake in WAT and BAT were decreased on a per gram basis, although the substantial increase in adipose tissue mass likely made

total uptake in BAT and WAT of desnutrin-ASKO mice higher, consistent with our finding of no net change in whole body glucose uptake (Figure S2D and E, middle and right). However, hepatic insulin sensitivity was markedly improved in desnutrin-ASKO mice. Hepatic glucose production was 16% lower under basal conditions and 76% lower during the clamp (Figure S2F, left). While there was no suppression of hepatic glucose production in flox/flox mice, there was a 77 % suppression in desnutrin-ASKO mice (Figure S2F, right), consistent with our findings of decreased ectopic TAG storage in the liver. To understand the possible cause of the improved hepatic insulin sensitivity, we measured total cellular hepatic DAG levels. We found that cytosolic DAG levels, which have been positively correlated with insulin resistance were markedly decreased in the livers of desnutrin-ASKO mice (Figure S2H-I) (Samuel et al., 2010). Taken together, these findings indicate that, despite increased adiposity, impaired adipocyte lipolysis in desnutrin-ASKO mice leads to decreased circulating FA levels preventing ectopic TAG storage in the liver and decreasing DAG levels, thereby improving hepatic insulin sensitivity.

Inhibition of lipolysis results in massive TAG accumulation in WAT and BAT of desnutrin-ASKO mice. However, as a result of blunted adipocyte lipolysis, ectopic TAG storage in the liver of these mice is prevented, even on a HFD. In this regard, desnutrin-ASKO mice represent a unique model, exhibiting increased adiposity yet protection from ectopic TAG storage. Our findings are in contrast to those mice with globally ablated desnutrin/ATGL that exhibit massive TAG accumulation in multiple organs, including the liver (Haemmerle et al., 2006). However, both global ablation and adipose-specific ablation of desnutrin result in enhanced insulin sensitivity, suggesting desnutrin deficiency in adipose tissue probably brings an increase in insulin sensitivity. Studies on glucose/insulin homeostasis in global desnutrin null mice have reported conflicting results, with some showing enhanced hepatic insulin sensitivity while others showing impaired insulin signaling in the liver (Kienesberger et al., 2009; Turpin et al., 2010). A major limitation of these studies is that hyperinsulinemic euglycemic clamps were not possible, because these mice die early and could not survive the procedure (Turpin et al., 2010). Here, we show by hyperinsulinemic euglycemic clamp studies that desnutrin-ASKO mice exhibit improved hepatic insulin sensitivity with resistance to ectopic fat storage, even on a HFD (Turpin et al., 2010). Moreover, we demonstrate that this improved hepatic sensitivity is probably due to lower DAG levels, which have been shown to affect insulin signaling (Samuel et al., 2010).

Figure S3. Similar embryonic BAT morphology of desnutrin-ASKO and flox/flox mice. A) Transmission electron microscopy from BAT of flox/flox and desnutrin-ASKO mice at E17 showing the lipid droplet (upper) or focusing on mitochondria (lower). Scale bar upper=1μM, scale bar below=0.5μM. B) Transmission electron microscopy from BAT of flox/flox and desnutrin-ASKO mice at E21 showing the lipid droplet (upper) or focusing on mitochondria (lower). Scale bar upper=1μM, scale bar below=0.5μM.

Figure S4. Effect of AMPK activators on desnutrin levels and lipolysis. A) Western blot, using a desnutrin-specific antibody, for endogenous desnutrin and desnutrin-HA-GFP, from lysates (10μg) of differentiated 3T3-L1ΔCAR adipocytes infected with desnutrin-HA-GFP or GFP control and treated with or without AICAR (2mM) in the

experiment performed in Figure 4J *, Non-specific bands. B) Western blot, using a HA and control GAPDH antibody, of lysates (10μg) of 3T3-L1ΔCAR adipocytes infected with WT desnutrin-HA-GFP, S406A mutant or GFP control and treated with or without Metformin (0.5mM) for 15h. C) FA release from 3T3-L1ΔCAR adipocytes infected with WT desnutrin and S406A mutant treated with or without AICAR (2mM) or Metformin (0.5mM) for 4h. D) Western blot for phospho-AMPK (T172) and total AMPK from lysates (20μg) of 3T3-L1ΔCAR adipocytes treated with or without AICAR (2mM) or Metformin (0.5mM) for 4h. E) RT-qPCR for the expression of HSL and desnutrin in 3T3-L1ΔCAR adipocytes (n=6). F) FA release from HEK 293 cells preloaded with oleic acid, transfected with desnutrin, and treated with or without AICAR (1μM) for 6h. G) Glucose levels during AICAR or DMSO injection taken at 0 hr and 5 hrs after injection. 20 week old flox/flox or desnutrin-ASKO mice were injected intraperitoneally with AICAR (0.5mg/g of body weight) or DMSO (vehicle). Food was removed at the start of the experiment. Glucose was also injected in all groups of mice (2mg/g of body weight) to prevent hypoglycemia from AICAR injection. Blood glucose was measured at 0 and 5 hrs after. Data are expressed as means ± SEM. $*P < 0.05$, $***P < 0.001$.

Levels of endogenous desnutrin and desnutrin overexpressed by CMV-promoter were unchanged in cells treated with AICAR (during the experimental period shown in Figure 4J) or Meformin in 3T3-L1ΔCAR adipocytes infected with desnutrin-HA-GFP or GFP control adenovirus (Figure S4A and B). Likely due to the high level of HSL, which is inhibited by AMPK, in comparison to desnutrin (Figure S4E), AICAR or Metformin treatment for 4 hrs decreased lipolysis in control-GFP infected 3T3-L1ΔCAR adipocytes (data not shown). However, adenovirus-mediated overexpression of WT desnutrin caused 1.5 to 1.6-fold increase in lipolysis over control-GFP infected cells in basal non-treated cells, whereas AICAR or Metformin treatement caused a 2.9 or 2.4-fold increase in lipolysis, respectively. This increase in lipolysis under both basal and AMPK-activated conditions, was not observed in cells overexpressing S406A mutant (Figure S4C), indicating that phosphorylation of desnutrin at S406 by AMPK activates desnutrin-catalyzed lipolysis. Moreover, in HEK 293 cells that express a very low level of endogenous lipases, overexpression of desnutrin caused increase in lipolysis upon 4 hr treatment with AICAR (Figure S4F).

SUPPLEMENTAL REFERENCES

Ahmadian, M., Duncan, R.E., Varady, K.A., Frasson, D., Hellerstein, M.K., Birkenfeld, A.L., Samuel, V.T., Shulman, G.I., Wang, Y., Kang, C., and Sul, H.S. (2009). Adipose overexpression of desnutrin promotes fatty acid use and attenuates diet-induced obesity. Diabetes 58, 855-866.

Duncan, R.E., Wang, Y., Ahmadian, M., Lu, J., Sarkadi-Nagy, E., and Sul, H.S. (2009). Characterization of desnutrin functional domains:Critical residues for triacylglycerol hydrolysis in cultured cells. J Lipid Res 51, 309-17.

Folch, J., Lees, M., and Sloane Stanley, G.H. (1957). A simple method for the isolation and purification of total lipides from animal tissues. J Biol Chem 226, 497-509.

Haemmerle, G., Lass, A., Zimmermann, R., Gorkiewicz, G., Meyer, C., Rozman, J., Heldmaier, G., Maier, R., Theussl, C., Eder, S., Kratky, D., Wagner, E.F., Klingenspor, M., Hoefler, G., and Zechner, R. (2006). Defective lipolysis and altered energy metabolism in mice lacking adipose triglyceride lipase. Science 312, 734-737.

Kim, K.H., Lee, K., Moon, Y.S., and Sul, H.S. (2001). A cysteine-rich adipose tissue-specific secretory factor inhibits adipocyte differentiation. J Biol Chem 276, 11252-11256.

Kienesberger, P.C., Lee, D., Pulinilkunnil, T., Brenner, D.S., Cai, L., Magnes, C., Koefeler, H.C., Streith, I.E., Rechberger, G.N., Haemmerle, G., Flier, J.S., Zechner, R., Kim, Y.B., and Kershaw, E.E. (2009). Adipose triglyceride lipase deficiency causes tissue-specific changes in insulin signaling. J Biol Chem 284, 30218-30229.

Latasa, M.J., Griffin, M.J., Moon, Y.S., Kang, C., and Sul, H.S. (2003). Occupancy and function of the -150 sterol regulatory element and -65 E-box in nutritional regulation of the fatty acid synthase gene in living animals. Mol Cell Biol 23, 5896-5907.

Neschen, S., Morino, K., Hammond, L.E., Zhang, D., Liu, Z.X., Romanelli, A.J., Cline, G.W., Pongratz, R.L., Zhang, X.M., Choi, C.S., Coleman, R.A., and Shulman, G.I. (2005). Prevention of hepatic steatosis and hepatic insulin resistance in mitochondrial acyl-CoA:glycerol-sn-3-phosphate acyltransferase 1 knockout mice. Cell Metab 2, 55-65.

Orlicky, D.J., DeGregori, J., and Schaack, J. (2001). Construction of stable coxsackievirus and adenovirus receptor-expressing 3T3-L1 cells. J Lipid Res 42, 910-915.

Samuel, V.T., Choi, C.S., Phillips, T.G., Romanelli, A.J., Geisler, J.G., Bhanot, S., McKay, R., Monia, B., Shutter, J.R., Lindberg, R.A., Shulman, G.I., and Veniant, M.M. (2006). Targeting foxo1 in mice using antisense oligonucleotide improves hepatic and peripheral insulin action. Diabetes 55, 2042-2050.

Samuel, V.T., Petersen, K.F., and Shulman, G.I. (2010)Lipid-induced insulin resistance: unravelling the mechanism. Lancet 375, 2267-2277.

Turner, S.M., Murphy, E.J., Neese, R.A., Antelo, F., Thomas, T., Agarwal, A., Go, C., and Hellerstein, M.K. (2003). Measurement of TG synthesis and turnover in vivo by 2H2O incorporation into the glycerol moiety and application of MIDA. Am J Physiol Endocrinol Metab 285, E790-803.

Turpin, S.M., Hoy, A.J., Brown, R.D., Garcia Rudaz, C., Honeyman, J., Matzaris, M., and Watt, M.J. (2010)Adipose triacylglycerol lipase is a major regulator of hepatic lipid metabolism but not insulin sensitivity in mice. Diabetologia, 146-156.

Villena, J.A., Hock, M.B., Chang, W.Y., Barcas, J.E., Giguere, V., and Kralli, A. (2007). Orphan nuclear receptor estrogen-related receptor alpha is essential for adaptive thermogenesis. Proc Natl Acad Sci U S A 104, 1418-1423.

Yu, C., Chen, Y., Cline, G.W., Zhang, D., Zong, H., Wang, Y., Bergeron, R., Kim, J.K., Cushman, S.W., Cooney, G.J., Atcheson, B., White, M.F., Kraegen, E.W., and Shulman, G.I. (2002). Mechanism by which fatty acids inhibit insulin activation of insulin receptor substrate-1 (IRS-1)-associated phosphatidylinositol 3-kinase activity in muscle. J Biol Chem 277, 50230-50236.

Samuel, V.T., Petersen, K.F., and Shulman, G.I. (2010)Lipid-induced insulin resistance: unravelling the mechanism. Lancet 375, 2267-2277.

SUPPLEMENTAL EXPERIMENTAL PROCEDURES

Generation of desnutrin floxed mice

A desnutrin targeting vector was constructed to introduce loxP sites upstream and downstream of exon1 which contains its translation start site and catalytic domain. The pFlexible plasmid containing the puromycin resistance gene (pFlex) (provided by Allan Bradley) was used for construction of the desnutrin targeting vector. FRT sites flanking the puromycin resistance gene facilitates its removal by Flp Recombinase and loxP sites facilitate removal of the targeted exon1 by Cre recombinase. The desnutrin sequence, amplified by PCR from 129/SV genomic DNA was cloned into pFlex. For the 5' homology arm, a 1.92 kb fragment containing the desnutrin promoter was amplified by PCR introducing Asc1 restriction sites at both the 5' and 3' ends and cloned into the Asc1site of pFlex. For the conditional arm, a 1.56 kb fragment containing part of the desnutrin promoter and exon1 was amplified by PCR introducing a HindIII site at the 5' end and a PacI site at the 3' end and cloned into HindIII-PacI digested pFlex with the inserted 5' homology arm. For the 3' homology arm, a 3.6 kb fragment containing intron 1 through exon 7 was amplified by PCR introducing NotI sites at both the 5' and 3' ends and cloned into the NotI site of pFlex with 5' homology and conditional arms. The resulting targeting vector was digested with PmeI and electroporated into 129/SvJ E14 ES cells. The cells were selected by maintenance in puromycin-containing media. ES cell clones with the desired homologous recombination event were identified by PCR, microinjected into 3.5-day blastocysts derived from C57BL/6 females, and transferred to pseudopregnant C57BL/6 recipients. Chimeric mice were then bred with C57BL/6 mice for germline transmission. The presence of the targeted allele in the agouti-colored offspring was confirmed by PCR. These mice were then mated with mice expressing FLP recombinase driven by the human ACTB promoter (Jackson laboratory) to excise the puromycin resistance gene to generate desnutrin flox/+ mice that were identified by PCR using primer sequences flanking the puromycin resistance gene and FRT sites. Homozygous desnutrin flox/flox mice were crossed with transgenic mice expressing Cre recombinase under the control of the aP2 promoter (Jackson Laboratory). Offspring inheriting both the targeted allele and the Cre transgene (aP2-Cre-desnutrin flox/+) were crossed with desnutrin flox/flox mice to yield desnutrin flox/flox Cre adipose-specific knockout mice (desnutrin-ASKO). Adipose tissue specific knockout for the desnutrin gene, removal of exon 1, was verified by PCR with primer sequences flanking exon 1 and loxP sites using DNA extracted from adipose tissue with a DNeasy kit (Qiagen).

Mouse maintenance

All studies received approval from the University of California at Berkeley Animal Care and Use Committee. We compared desnutrin-ASKO and flox/flox littermates on a C57BL/6J background. PPARα null mice were obtained from Jackson laboratory (Bar Harbor, ME, USA). We provided either a standard chow or a HFD (HFD; 45% of kcal from fat, 35% of kcal from carbohydrate and 20% of kcal from protein, Research Diets) *ad libitum*. For tail vein injection of adenovirus, WT C57BL/6J were fed a HFD for 3 wks and then injected with WT desnutrin, S406A mutant or control GFP virus ($1x10^9$ plaque forming units/mouse). All studies, unless indicated were performed on HFD- fed mice.

GST pull-down assay

GST-fusion proteins were expressed in the *Escherichia coli* strain BL21(DE3)pLysS. Bacteria were grown to an OD_{600} of 0.5, and the expression of fusion protein was induced for 2 h by adding isopropyl 1-thio-ß-D-galactopyranoside to a final concentration of 0.5 mM. Bacteria expressing GST and GST-14–3-3 were harvested by centrifugation and resuspended in 10 mM phosphate buffer, pH 7.4, 140 mM NaCl, 3 mM KCl, 1 mM dithiothreitol (DTT), 50 mM NaF, 0.5% protease inhibitor. The suspension was sonicated 3x10 sec pulses for 5 min. The resulting lysate was cleared by centrifugation and used directly in GST pull-down experiments. [^{35}S]Methionine-labeled desnutrin and desnutrin mutants were synthesized *in vitro* using TnT-coupled reticulocyte lysate (Promega Corp., Madison, WI). GST-fusion protein (50 µg) was incubated with 40 µl glutathione agarose beads, 50 µl of *in vitro* translated protein in 1ml PBS binding buffer (PBSB) (20 mM HEPES-KOH, pH 7.9, 10% (vol/vol) glycerol, 100 mM KCl, 5 mM $MgCl_2$, 1 mM EDTA, 50mM NaF, 0.5% protease inhibitor cocktail) overnight at 4°C. The beads were recovered by centrifugation and washed twice with PBSB, twice with PBS, and bound proteins were eluted by SDS-PAGE sample buffer, analyzed on SDS-PAGE, and visualized by autoradiography. To dephosphorylate the *in vitro* translated desnutrin protein, 50 µl of translation reaction were incubated in the presence or absence of 5 U of alkaline phosphatase (Roche) in 50 mM Tris-HCl, pH 8.5, 0.1 mM EDTA at 37°C for 1 h. The reactions were subsequently used in GST pull-down experiments.

Immunoblotting

Total lysates were subjected to 10% SDS-PAGE, transferred to nitrocellulose membranes, and probed with rabbit anti-desnutrin antibody that we generated, anti-GAPDH (Santa Cruz), anti-UCP-1 (Sigma), anti-phospho-AMPK Thr172, anti-AMPK, anti-phospho-ACC Ser79, anti-ACC, anti-phospho-(Ser) 14-3-3 binding motif (Cell Signaling), anti-HA (Covance) or anti-Myc (Millipore) primary antibodies followed by horseradish peroxidase conjugated secondary antibody (Biorad). Blots were visualized using enhanced chemiluminescence substrate (PerkinElmer) and images were captured using a Kodak Image Station 4000MM.

Immunoprecipitation

HEK 293 cells were transfected with WT desnutrin-HA-GFP and then treated with either DMSO, 20 µM compound C (Calbiochem), 1 mM AICAR (Toronto Research), or 20 µM compound C with 1 mM AICAR for 1 h before lysis. HEK 293 cells were also co-transfected with desnutrin tagged with HA-GFP, and Myc-tagged 14-3-3. Lysates from the transfected HEK 293 cells and WAT were prepared in 1% Triton-X-100, 150 mM NaCl, 10% glycerol, 25 mM Tris, pH 7.4, 0.05 M NaF and protease inhibitor cocktail (Sigma) and then were centrifuged at 4°C for 20 min at 12,000 g. Lysates were then rotated overnight at 4°C with antibodies to either HA (Covance) or desnutrin followed by addition of 40 µl of protein A/G agarose beads (Santa Cruz) for 1 h. Beads were collected by pulse centrifugation and washed 4 times with lysis buffer prior to resolution by SDS-PAGE and immunoblotting.

Chromatin immunoprecipitation

BAT isolated as previously described (Villena et al., 2007) fixed with 2mM

disuccinimidyl glutarate for 45 min at room temperature before 2% formaldehyde crosslinking for 30 min. ChIP was performed as previously described (Latasa et al., 2003) using GAPDH, PPARα and RIP140 antibodies (Santa Cruz) and primers to the UCP-1 enhancer (Fow:AGCTTGCTGTCACTCCTCTACA, Rev:TGAGGAAAGGGTTGACCTTG).

***In vitro* kinase assay**

HEK 293 cells were transfected with either GFP, WT desnutrin-HA-GFP or mutant forms of desnutrin S406A-HA-GFP and S430A-HA-GFP, immunoprecipitated with HA conjugated beads (Sigma) and then incubated with purified AMPKα1 (Millipore) in a buffer containing 5 mM HEPES, pH 7.5, 0.1 mM dithiothreitol, 0.25% NonidetP-40, 7.5 mM $MgCl_2$, 50 μM ATP, 5 μCi of [γ-^{32}P]ATP and incubated for 30 min at 30°C. Reactions were stopped with the addition of 2x SDS loading buffer. The protein products were separated on SDS-PAGE, transferred to nitrocellulose membranes, which were then subjected to autoradiography and western blot analysis using an anti-HA antibody (Covance) or an anti-phospho-(Ser) 14-3-3 binding motif antibody (Cell Signaling).

***In vitro* TAG hydrolase assay**

Lysates were prepared from HEK 293 cells overexpressing WT desnutrin-HA-GFP, mutant desnutrin S406A-HA-GFP or mutant desnutrin S406D-HA-GFP by lysis in 50mM Tris, pH 7.4, 0.1 M sucrose, and 1 mM EDTA, followed by centrifugation at 9,000 g for 15 min at 4°C. Lysates from livers of adenovirus infected mice or from BAT of flox/flox and desnutrin-ASKO mice were prepared in the same assay buffer. Reactions were started by addition of supernatants containing 100 μg of protein in 100 μl volumes to 100 μl of substrate containing 2X concentrations of [^{3}H] triolein (75 μM), sonicated into mixed micelles with 25 μM egg yolk lecithin, 100 μM taurocholate, 2% BSA (w/v), 1 mM DTT, and 50 mM potassium phosphate, pH 7.2. Reactions were allowed to proceed for 1h at 37°C and were terminated by the addition of 3.5 ml of methanol:chloroform:heptane (10:9:7). FAs were extracted with 1 ml of 0.1 M potassium carbonate, 0.1 M boric acid, pH 10.5, and radioactivity in 1 ml of upper phase obtained after centrifugation for 20 min at 800x g was quantified by scintillation counting. Radioactivity in GFP control samples was taken as a baseline of TAG hydrolase activity in lysates and subtracted from test values.

Lipolysis

Gonadal fat pads or BAT from overnight fasted mice were cut into 50 mg samples and incubated at 37ºC without shaking in 500ul of KRB (12 mM HEPES, 121mM NaCl, 4.9 mM KCl, 1.2 mM $MgSO_4$ and 0.33 mM $CaCl_2$) containing 2% FA free BSA and 0.1% glucose with or without 10 μM isoproterenol. FA and glycerol release were measured in aliquots from incubation buffer using the NEFA C Kit (Wako) and Free Glycerol Reagent (Sigma), respectively. For lipolysis in transfected cells, HEK 293 cells were plated in 6 well plates and transfected with either GFP, WT desnutrin-HA-GFP or mutant desnutrin S406A-HA-GFP. Four hours later the transfection medium was removed and the cells were treated with growth medium containing 300μM oleic acid, 1% FA free BSA, 0.5 μg/ml insulin for 16h. The cells were rinsed once with KRB supplemented with 4% FA free BSA and then incubated in this media overnight with or without 1 mM

AICAR (Toronto Research Chemicals). 3T3-L1CARΔ cells (D. Orlicky, University of Colorado Cancer Center) were differentiated as previously described (Kim et al., 2001; Orlicky et al., 2001; Ahmadian et al., 2009b). Differentiated adipocytes were infected with adenovirus containing control GFP, WT desnutrin-HA-GFP or mutant desnutrin S406A-HA-GFP that we previously generated (Duncan et al., 2009). Once overexpression was verified, media was changed to KRB buffer with or without 2mM AICAR for 12 h, media was then changed to KRB without AICAR and aliquots were removed from the media 8 h later FA measurements.

Adipocyte size determination

Gonadal fat samples and intrascapular BAT were fixed in 10% buffered formalin, embedded in paraffin, cut into 8 μm-thick sections, and stained with hemotoxylin and eosin. Adipocyte size was determined with Image J software (US National Institutes of Health), measuring a minimum of 300 cells per sample.

Adipocyte isolation

Gonadal fat pads or BAT were digested for 1 h at 37ºC with collagenase (Sigma) in Krebs-Ringer Buffer (KRB; 12 mM HEPES, 121 mM NaCl, 4.9 mM KCl, 1.2 mM $MgSO_4$ and 0.33 mM $CaCl_2$) supplemented with 3 mM glucose and 1% FA free BSA, filtered through nylon mesh, centrifuged and adipocytes collected from the upper phase.

FA oxidation

FA oxidation in isolated adipocytes was determined by measuring $^{14}CO_2$ production from [U-^{14}C] palmitic acid (0.2 μCi/ml) after incubation for 1 h at 37ºC with gentle shaking. The buffer was acidified with 0.25 ml of H_2SO_4 (5N), and maintained sealed at 37ºC for an additional 30 min. Trapped radioactivity was quantified by scintillation counting.

Transmission electron microscopy

BAT and WAT were fixed in 2% glutaraldehyde in 0.1 M PB (phosphate buffer), pH 7.3 at 4°C overnight; then postfixed in 1% OsO_4 and embedded in an Epon-Araldite mixture. Ultrathin sections (0.2 μm) mounted on 150-mesh copper grids were stained with lead citrate and observed under a FEI Tecnai 12 transmission electron microscope.

Cryosectioning

Fresh liver and adipose tissue from 16-week old mice fed a HFD were rinsed with PBS, then embedded in OCT medium and snap-frozen. The specimen was cut while frozen into slices at 8 μm in a cryotome and fixed with a 10% formaldehyde solution. The formaldehyde was rinsed with water and dehydrated with 50%, 70%, 85%, 95% and 100% ethanol. The sections were stained with freshly prepared Oil Red O working solution (0.5%) for 15 min and subsequently rinsed with 60% isopropanol. The nuclei were then lightly stained with hematoxylin for 30 sec and rinsed with water and mounted in aqueous mountant.

Blood and tissue metabolites

Fasting serum triglycerides and FAs were analyzed with Infinity Triglyceride reagent (Thermo Trace) and NEFA C kit (Wako), respectively. Serum insulin was determined

using an enzyme–linked immunosorbent assay kit (Alpco).

$^{2}H_2O$ labeling and GCMS analysis of TAG-glycerol and TAG-FA

The heavy water ($^{2}H_2O$) labeling protocol and GCMS analyses of TAG-glycerol and TAG-FA from adipose tissue have been described previously in detail (Turner et al., 2003). Mice were intraperitoneally injected with 100% $^{2}H_2O$, 0.9% NaCl (0.025 ml/g body weight) and administered $^{2}H_2O$ in drinking water starting at 20 weeks of age for a 6 day period after which lipids were extracted from gonadal fat pads by the Folch method (Folch et al., 1957) for subsequent analysis.

Calculation of all-source TAG turnover

Fractional TAG-glycerol synthesized from glycerol phosphate during the period of $^{2}H_2O$ administration was measured as described (Turner et al., 2003):

$$f\text{TAG} = \text{EM1}_{\text{TAG-glycerol}}/\text{A1}_{\text{TAG-glycerol}}$$

EM1 is the measured excess mass isotopomer abundance for M1-glycerol at time t and A1 is the asymptotic mass isotopomer abundance for M1-glycerol, assuming that four of five C-H bonds of glycerol phosphate are replaced by H-atoms from tissue water (Turner et al., 2003).

Calculation of de novo palmitate turnover

Fractional contributions from de novo lipogenesis (DNL) were calculated using a combinatorial model as previously described (Turner et al., 2003):

$$f\text{DNL} = \text{EM1}_{\text{FA}}/\text{A1}_{\text{FA}}$$

where *f*DNL represents the fraction of total TAG-palmitate in the depot derived from DNL during the labeling period. The fraction of newly synthesized TAG-palmitate from DNL is also calculated by correcting the measured fractional contribution from DNL (*f*DNL) for the degree of replacement of adipose TAG during the labeling period:

DNL contribution to newly synthesized TAG=*f*DNL/*f*TAG

Hyperinsulinemic-euglycemic clamp

We implanted jugular venous catheters seven days prior to the study. After an overnight fast, we infused [3-^{3}H] glucose (Perkin Elmer) at a rate of 0.05 μCi/min for 2 hours to assess basal glucose turnover, followed by the hyperinsulinemic-euglycemic clamp for 140 min with a primed/continuous infusion of human insulin (154 pmol/kg prime (21 mU/kg)) over 3 min, followed by 17 pmol/kg/min (3 mU/kg/min) infusion (Novo Nordisk), a continuous infusion of [3-^{3}H] glucose (0.1 μCi/min), and a variable infusion of 20% dextrose to maintain euglycemia (100–120 mg/dl). We obtained plasma samples from the tail and measured tissue-specific glucose uptake after injection of a bolus of 10μCi of 2-deoxy-D-[1-^{14}C]glucose (Perkin Elmer) at 85 min. We analyzed our results as previously described (Samuel et al., 2006).

TAG and DAG extraction

For TAG quantification, total neutral lipids were extracted by the method of Folch (Folch et al., 1957). Lipids were solubilized in 1% tritonX-100 and TAG was measured using Infinity Reagent (Thermo). DAG extraction and analysis in both cytosolic and membrane samples from quadriceps muscle and liver tissue was performed as previously described (Neschen et al., 2005; Yu et al., 2002). Total DAG content was expressed as the sum of individual DAG species.